

TECHNICAL SCIENCES

OPTIMIZATION OF TECHNOLOGICAL PARAMETERS OF PULSED ARC MIG WELDING OF Al–Mg–Mn 1561 ALLOY

Zhao Yu.

China-Ukraine Institute of Welding, Guangdong Academy of Sciences, Guangdong Provincial Key Laboratory of Material Joining and Advanced Manufacturing, Guangzhou, China

Illiashenko Ye.

E.O. Paton Electric Welding Institute, National Academy of Sciences of Ukraine Kyiv, Ukraine

Wang X.

China-Ukraine Institute of Welding, Guangdong Academy of Sciences, Guangdong Provincial Key Laboratory of Material Joining and Advanced Manufacturing, Guangzhou, China

Konoreva O.,

Alyoshin A. (junior),

Shevchenko V.,

Popov Ye.,

Yarosh V.

E.O. Paton Electric Welding Institute, National Academy of Sciences of Ukraine Kyiv, Ukraine

ABSTRACT

This study examines the influence of technological parameters (welding speed and heat input) in pulsed-arc MIG welding on the microstructure, microhardness, and mechanical properties of butt joints of the aluminum alloy Al–Mg–Mn 1561. A series of experiments was conducted at various welding speeds (380, 500, and 600 mm/min) with corresponding heat input values. Metallographic analysis, tensile testing, and microhardness measurements were conducted. It was found that increasing the welding speed and decreasing the heat input not only resulted in grain refinement in the weld zone and fusion lines, but also reduced the size of porosity. The microhardness of the weld increased to 780 MPa, and the tensile strength of the joint reached ≈ 360 MPa ($\approx 86\%$ of the base metal strength). The results obtained indicate that the welding mode $V = 600$ mm/min and $E \approx 217$ J/mm is optimal for the 1561 alloy. These results can be used to optimize the welding technology of aluminum alloys in mechanical engineering and aviation.

Keywords: pulsed-arc metal inert gas (MIG) welding, aluminum alloy 1561, welding modes, microstructure, strength.

Introduction. Aluminum alloys of the Al–Mg–Mn system are among the most widely used materials in transport engineering, aviation, and the energy industry. Their thermophysical properties, namely high specific strength in combination with good corrosion resistance and workability, as well as high thermal and electrical conductivity, are key advantages that have led to the increasing use of these materials in the automotive industry. Furthermore, aluminum alloys are readily processable, which further facilitates their continued application in various industrial sectors [1–3]. Specifically, alloy 1561 (analogue to 5083 or $\text{AlMg}_{4.5}\text{Mn}_{0.7}$) exhibits enhanced strength, weldability, and resistance to intergranular corrosion [4, 5]. MIG welding is a welding method that utilizes an inert gas to shield the weld metal from contamination. It offers advantages such as high welding speed, high weld quality, simple operation, high productivity, and high efficiency [6]. However, welding of aluminum alloys presents several technological challenges: high thermal conductivity leads to significant heat loss and unstable penetration; low hydrogen solubility contributes to porosity formation in the weld metal; Thermal exposure leads to grain coarsening, loss of strength, and the formation of a softening zone in the heat-affected zone (HAZ) [7–10]. Optimization of welding modes, particularly pulsed-arc MIG welding, enables control of heat input, reduces overheating, and stabilizes weld formation [11,

12]. It is well established that welding parameters—including torch travel speed, welding current, arc voltage, pulse frequency, and linear heat input—have a decisive impact on weld morphology, structure, porosity, and joint strength [13–15].

A number of studies have focused on evaluating the influence of welding modes on the structure and properties of Al–Mg–Mn aluminum alloys. The authors of [16] established the trends of structure formation in welded joints of the 1561 aluminum alloy, 4 mm in thickness, as a function of changes in MIG welding parameters on a steel substrate, selecting the modes based on the criterion of satisfactory weld formation. They identified the optimal welding mode according to the criteria of minimizing pore formation, refining grain structure, and enhancing mechanical properties. Increasing MIG welding speed promotes grain refinement in the weld, decreases their aspect ratio, and simultaneously increases the number of pores while reducing their size.

Despite the existence of numerous studies on aluminum alloys, research specifically on the 1561 alloy under variable-speed pulsed MIG welding remains limited. In particular, there is a lack of comprehensive data on the relationship between welding speed, heat input, microstructure, and weld strength. Therefore, it is necessary to conduct a systematic experimental study to

improve the reliability and durability of the joints of this alloy.

The objective of this work is to identify the regularities of the effect of welding speed and heat input in pulsed-arc MIG welding on the microstructure, defect formation, and mechanical properties of butt joints of the Al–Mg–Mn 1561 alloy.

To achieve the objective, the following tasks have been defined:

1. To establish the patterns of macrostructure formation in weld seams as a function of welding speed and heat input.
2. To investigate the microstructural changes in butt joints of the 1561 alloy under the influence of welding speed and heat input.
3. To determine the distribution of microhardness and its dependence on technological parameters.
4. To assess the mechanical properties of welded joints and determine the optimal welding parameters.

Materials and Methods. In this study, a plate of 1561 aluminum alloy of the Al–Mg–Mn system with a

thickness of 4 mm is used as the base material. This alloy is characterized by enhanced corrosion resistance, high weldability in inert gas environments, and adequate ductility. The primary mechanical properties of alloy 1561 are: ultimate tensile strength – 335 MPa, yield strength – 185 MPa, and elongation of approximately 11%. Metallographic studies indicated that in the base metal 1561, the grain size ($D_g = h \times l$, where h is grain width and l is grain length) was $D_g = 7\text{--}10 \times 20\text{--}100\text{ }\mu\text{m}$, with a grain shape coefficient $\alpha = 3\text{--}10$ ($\alpha = l/h$). The microhardness of the base metal was HV 750–840 MPa.

Experiments were carried out using the MIG welding method, with ER5356 (AlMg5) electrode wire of 1.2 mm diameter and longitudinal butt welding of aluminum alloy plates measuring 300 mm × 100 mm × 4 mm. Argon of the highest grade (99.993%) was used as the shielding gas.

The chemical composition of 1561 alloy and ER5356 wire is presented in Table 1.

Table 1

Chemical composition of Al–Mg–Mn system materials used in the research

Materials	Chemical elements, wt.%									
	Al	Mg	Mn	Si	Fe	Cu	Zn	Zr	Cr	Ti
Base metal 1561	base	5.5–6.5	0.7–1.1	≤0.4	≤0.4	≤0.1	≤0.2	0.02–0.12	–	–
ER5356 welding wire	base	4.5–5.5	0.1–0.2	–	–	–	–	–	0.05–0.2	0.06–0.20

Prior to welding, the samples were prepared by scraping the surface to a width of 20–25 mm from the joint line and chemically etching in a 20% alkaline NaOH solution and a 15% nitric acid (HNO₃) solution. This treatment enabled the complete removal of the Al₂O₃ oxide film, which hinders the formation of a high-quality weld.

For the technological studies, a laboratory setup was assembled based on a MIG/MAG welding power source of the TPS 320i type (Fronius International GmbH, Austria) (Fig. 1).



Figure 1. External view of the laboratory setup for MIG welding of butt joints of the 1561 alloy

The butt joints were assembled using a special assembly-welding fixture with a stainless steel backing

plate featuring a 4×2.5 mm groove, ensuring the formation of root weld metal (Fig. 2).



Figure 2. 3D model (a) and photograph of the assembly-welding fixture for butt joints (b)

Metallographic studies were performed using a NEOPHOT-32 optical microscope (CARL ZEISS, Jena, Germany) in accordance with the methodology described in [17, 18]. To reveal the structure of the samples, etching was conducted: in an aqueous solution of NaOH followed by clarification with an aqueous solution of HNO_3 for macrostructure, and in an aqueous solution of hydrofluoric acid for microstructure [19]. For microstructural investigations, the recommendations and methodologies described in [18, 20, 21] were also used. The microhardness of the samples was measured by the Vickers method (HV) using an M400 microhardness tester ("LECO", St. Joseph, MI, USA) with a 100

gf load; the reported hardness values were averaged over three measurements [22]. To determine the strength of the specimens, static tensile tests were conducted using standard methodology on a universal servohydraulic testing system MTS 318.25 (MTS Systems Corporation, Eden Prairie, Minnesota, USA) with a maximum force of 250 kN. For all other investigations, comprehensive materials research methods were employed [23].

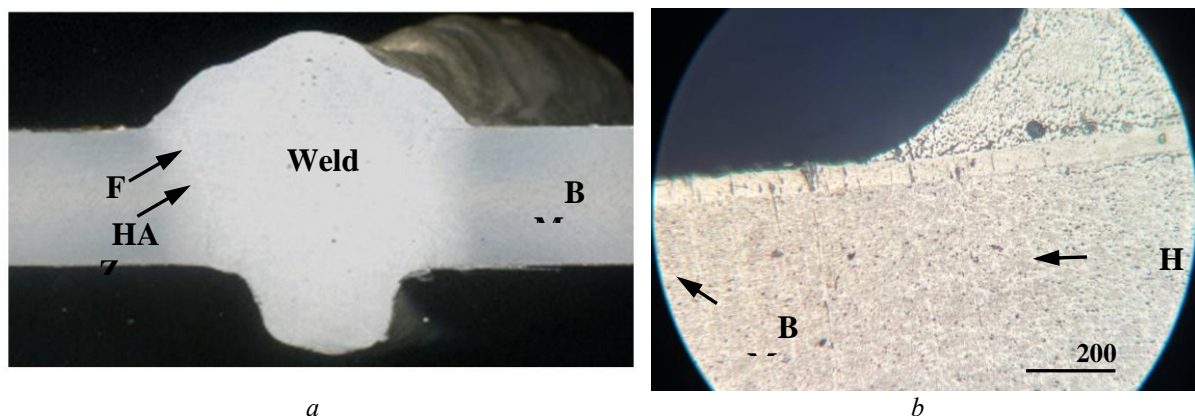
Research Results and Discussion. The parameters of the MIG welding modes for the 1561 alloy were selected based on the recommendations in [24–27] and following a series of experiments (Table 2).

Table 2

Parameters of welding modes for the 1561 alloy ($\delta=4$ mm)

Welding mode	Wire feed speed V_{wr} , m/min	Welding current I, A	Arc voltage U, V	Welding speed V, mm/min	Linear energy E, J/mm
No. 1	6.9	119	15.5	380	233
No. 2	8	137	18.2	500	240
No. 3	8.4	142	19.1	600	217

Figure 3 presents the macrostructure of welded joints of the 1561 alloy produced by MIG welding under various modes as specified in Table 2.



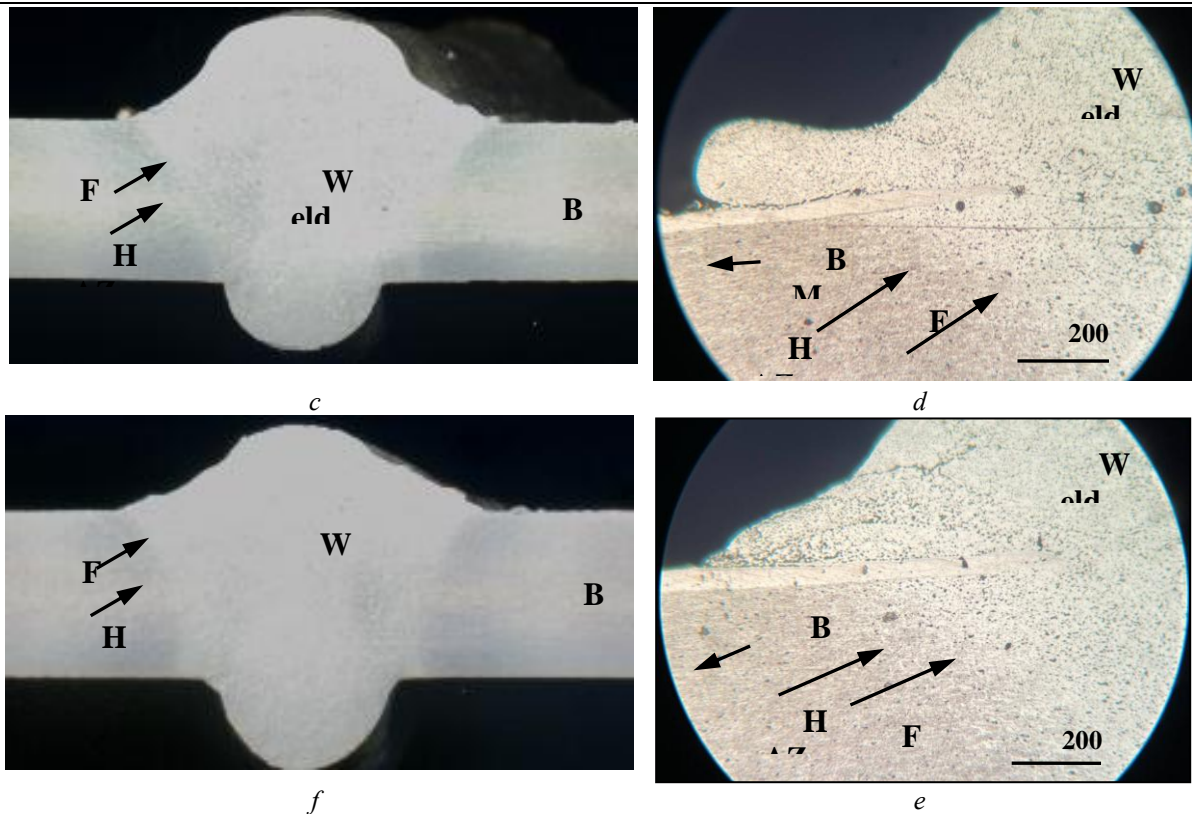


Figure 3. Macrosection (a, c, f) and general view of the weld (b, d, e) in the fusion line zone of welded joints of the 1561 alloy under different MIG welding modes ($\times 100$): a, b – mode No. 1; c, d – mode No. 2; e, f – mode No. 3 (BM – base metal, FL – fusion line, HAZ – heat-affected zone)

Investigation of the technological features of the MIG welding process for the 1561 alloy showed that all selected welding modes ensured satisfactory weld formation, in accordance with the requirements of ISO 10042 (quality levels from C to B) [28]. At the lowest speed (mode No. 1), slight bead thickening was observed due to excessive heat input. Increasing the speed

to 600 mm/min reduced the weld width and penetration depth, but resulted in a more uniform structure.

Metallographic studies of the microstructure of welded joints of the 1561 alloy under different MIG welding modes demonstrated that increasing the welding speed and decreasing the heat input led to a tendency for grain refinement and a transition from a dendritic to an equilibrium structure (Fig. 4).

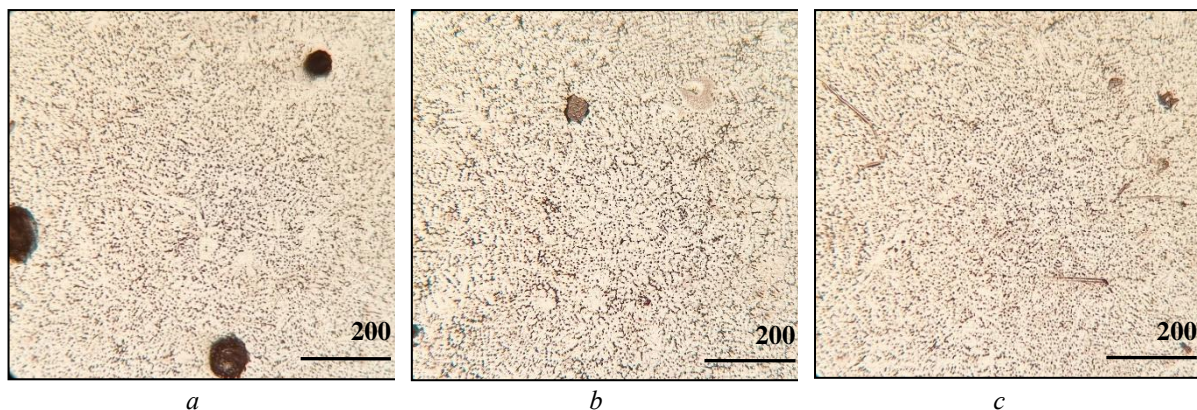


Figure 4. Microstructure of the weld metal of the 1561 alloy joint under different MIG welding modes ($\times 400$): a – mode No. 1; b – mode No. 2; c – mode No. 3

Metallographic analysis of the specimen obtained under welding mode No. 1 established that the weld metal is characterized by a mixture of elongated and equiaxed grains. The average grain size is $10\text{--}12 \times 30\text{--}100\text{ }\mu\text{m}$, with a grain shape coefficient of $\alpha = 3\text{--}8.3$. The structure contains pores with diameters of $60\text{--}230\text{ }\mu\text{m}$, predominantly located in the central part of the

weld (Fig. 4a). This structure is determined by the prolonged time the metal remains in the liquid state and the intensive evolution of hydrogen.

Upon examination of the specimen produced under welding mode No. 2, it is evident that the grains are finer ($10\text{--}15 \times 30\text{--}100\text{ }\mu\text{m}$) and more equiaxed, with the shape factor decreasing to $\alpha = 3\text{--}6.7$. The pores are

smaller in size (20–120 μm) and are observed less frequently (Fig. 4b). This indicates stabilization of the thermal cycle and a reduction in gas evolution intensity.

In the weld metal at welding mode No. 3, a fine-grained equiaxed structure (10–15 \times 30–70 μm) is formed, exhibiting the lowest grain aspect ratio, $\alpha = 3$ –4.7 (Fig. 4c). The pore diameter decreases to 20–40 μm . This indicates intensive cooling of the weld pool and a short crystallization phase, which promotes structural refinement.

In the fusion line zone, a gradual decrease in grain size and an increase in structural uniformity were observed with increasing welding speed. In welding mode No. 1, the grains exhibit an elongated shape measuring 10–30 \times 30–50 μm , while in mode No. 3 they measure only 10–15 \times 30–40 μm (Fig. 5).

In the heat-affected zone, the grains decrease on average by 1.5–1.7 times when transitioning from mode No. 1 to No. 3 (Fig. 5). A reduction of the grain shape coefficient (α) by 1.6 times is also observed, indicating intensive recrystallization during short-term heating.

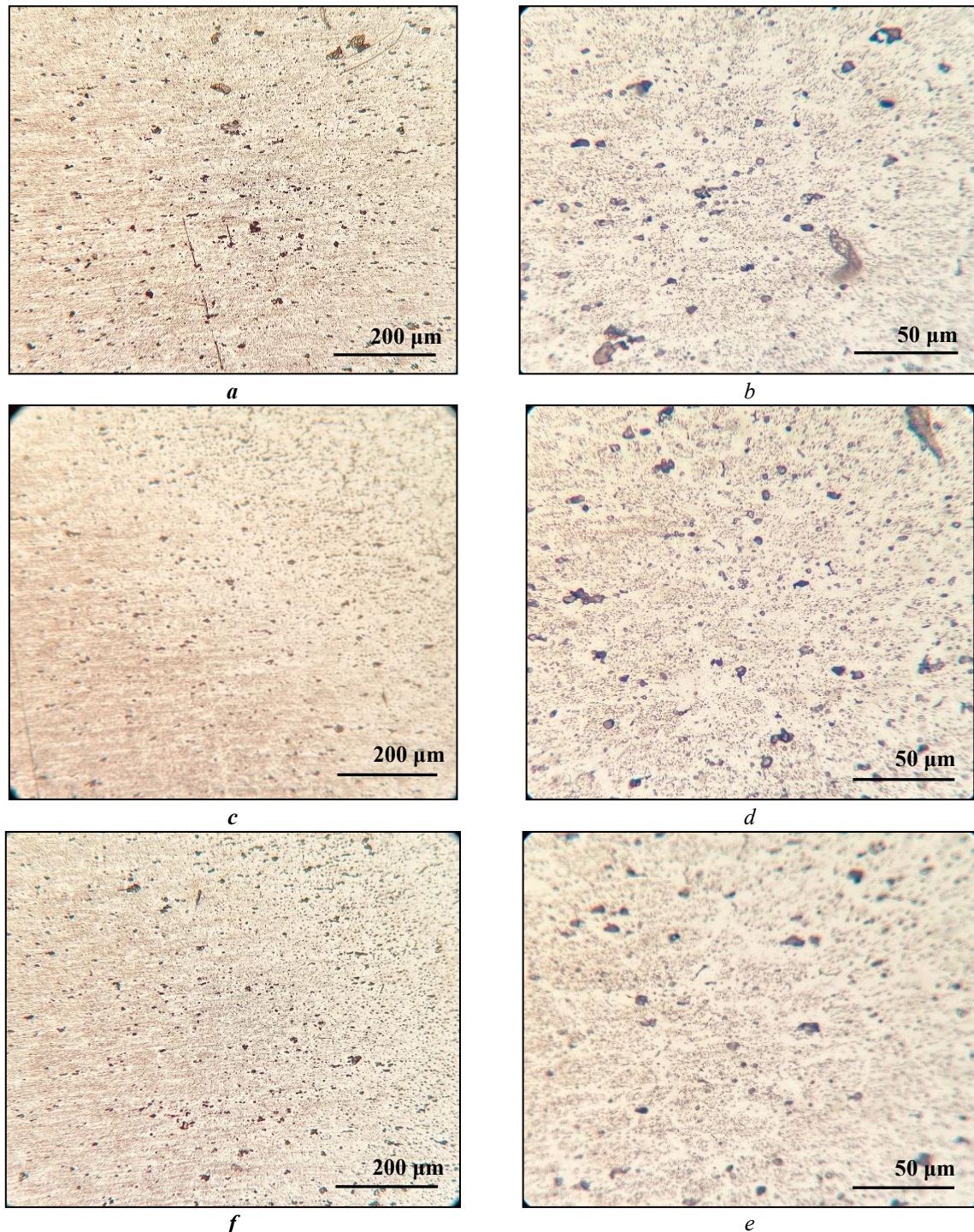


Figure 5. Microstructure of the metal at the fusion line (a, c, f, $\times 400$) and in the heat-affected zone (b, d, e, $\times 100$) of the 1561 alloy joint under different MIG welding modes: mode No. 1 (a, b); mode No. 2 (c, d); mode No. 3 (f, e)

Microhardness (HV) was measured across the welded joint. At welding mode No. 1, the microhardness of the weld was 640–680 MPa; at mode No. 2, it was 700–770 MPa; and at mode No. 3, it was 660–780 MPa. In the heat-affected zone, HV reached 740–860 MPa, which is attributed to partial strengthening due to thermal effects and local recrystallization.

With increasing welding speed, the average hardness increased by approximately 15% and the scatter of HV values decreased, indicating a more stable thermokinetic field during the process.

Tensile tests of welded joints of the 1561 alloy demonstrated that the ultimate strength (σ_B) and yield strength ($\sigma_{0.2}$) increase with increasing welding speed (Table 3).

Table 3

Mechanical properties of welded joints of the 1561 alloy as a function of MIG welding speed

Welding mode	V, mm/min	E, J/mm	$\sigma_{0.2}$, MPa	σ_B , MPa	δ , %	strength coefficient
No.1	380	233	250	300	9	0.70
No.2	500	240	280	330	10	0.78
No.3	600	217	305	360	11	0.86

The relative elongation (δ) increased from 9% to 11%, indicating improved ductility in conjunction with enhanced strength. Fracture of the specimens occurred along the fusion line, which is typical for aluminum alloys due to microdefects and the hardness gradient in this zone. The strength coefficient (the ratio of the $\sigma_{0.2}$ and σ_B values to BM, respectively) was lowest for the specimen obtained under welding mode No. 1 and highest (for the weld metal) for the specimen under welding mode No. 3. Thus, according to the mechanical tests conducted, it can be stated that superior mechanical properties of joints produced by MIG welding are achieved with reduced heat input and under conditions of high welding speed.

Research shows that increasing welding speed reduces the duration of thermal exposure and decreases the width of the thermal softening zone. At low welding speeds (380 mm/min), the weld zone forms under prolonged thermal exposure, which promotes recrystallization and grain coarsening. A decrease in heating time at a welding speed of 600 mm/min results in more intensive cooling and the predominance of an equiaxed structure, leading to increased hardness and strength.

High temperature and prolonged heating facilitate hydrogen diffusion and the formation of large pores (up to 230 μm). At higher cooling rates, fine pores are formed, which exert a lesser influence on the mechanical properties. Therefore, a fine-porous structure at high welding speed is more favorable than a coarse-porous structure at low speeds.

Microhardness closely correlates with grain size: refinement of crystallites leads to increased resistance to plastic deformation by the Hall–Petch mechanism. An increase in HV in the weld at a MIG welding speed up to 600 mm/min indicates the formation of a fine-grained equiaxed structure with a uniform distribution of Al–Mg–Mn phases.

The dependence of mechanical properties on MIG welding speed is nonmonotonic: at low speeds ($V \leq 400$ mm/min), a decrease in σ_B is observed due to overheating and the formation of coarse pores; at high welding speeds ($V \geq 600$ mm/min), improved strength is achieved through reduced heat input (217 J/mm) and grain refinement. A slight reduction in relative elongation ($\delta \approx 11\%$) indicates that ductility remains at a satisfactory level.

The obtained data indicate that the high-speed MIG welding mode ($V = 600$ mm/min, $E = 217$ J/mm) is optimal for the Al–Mg–Mn 1561 alloy, as it ensures the best balance between fine-grained structure, hardness, density, and joint strength.

Conclusions.

1. It has been established that increasing the welding speed from 380 to 600 mm/min, corresponding to a reduction in heat input from 240 to 217 J/mm, results in a significant improvement in weld formation. A decrease in heat input contributes to bead narrowing, arc stabilization, reduced penetration depth, and a smaller heat-affected zone. At low welding speeds (380 mm/min, $E \approx 240$ J/mm), the welds exhibit excessive penetration, bead thickening, and signs of overheating. The optimal welding speed range of 500–600 mm/min at $E = 215$ –225 J/mm ensures uniform weld geometry, absence of surface defects, and a stable crystallization process.

2. Metallographic studies indicate that increasing welding speed (while simultaneously reducing E) accelerates weld pool cooling, which promotes a transition from a columnar-dendritic to a fine-grained equiaxed structure. The grain size in the weld metal decreases from 10–12 \times 30–100 μm to 10–15 \times 30–70 μm , with the shape factor (α) decreasing from 8 to 4.7. Reducing heat input decreases the duration of the liquid phase and limits diffusion processes, resulting in a more uniform structure and less pronounced microsegregation of elements. In the fusion zone and heat-affected zone at a welding speed of 600 mm/min, a fine-grained structure is formed with isolated pores 20–40 μm in diameter (compared to 60–230 μm at 380 mm/min). Thus, increasing the speed and reducing the heat input are effective factors for grain refinement and porosity reduction.

3. As the welding speed increases from 380 to 600 mm/min (with a corresponding decrease in heat input from 240 to 217 J/mm), the average microhardness of the weld metal rises from 640–680 MPa to 660–780 MPa. In the heat-affected zone, hardness increases to 850 MPa, attributable to intensive cooling and the formation of fine-dispersed phases of the Al₆(Mn,Fe) type. At high heat input, localized softening occurs due to overheating and coagulation of strengthening particles. Thus, the microhardness of the weld is inversely proportional to the heat input and directly proportional to

the welding speed, which is consistent with the Hall–Petch relationship.

4. Tensile tests showed that with increasing welding speed and decreasing heat input, the ultimate tensile strength (σ_B) increases from 300 to 360 MPa, the yield strength ($\sigma_{0.2}$) from 250 to 305 MPa, and the elongation from 9 to 11%. The strength coefficient of the weld relative to the base metal reaches 0.86, indicating the high efficiency of the energetically balanced welding mode. The optimal combination of structural and mechanical properties is achieved at a welding speed of 600 mm/min and a linear heat input of approximately 217 J/mm. In this case, a fine-grained equiaxed structure with minimal porosity, uniform hardness distribution, and high strength with satisfactory ductility is formed.

Therefore, optimization of welding speed and heat input is a key factor in enhancing the quality of welded joints of the Al–Mg–Mn 1561 alloy. A reduction in heat input by 10–15% while maintaining stable penetration enables a 15–20% increase in weld strength without loss of ductility.

Acknowledgements.

The work was funded within the following programs:

1. The National Key Research and Development Program of China (Project Number: 2023YFE0201500).
2. National Key R&D Program of China [2020YFE0205300].

References

1. Olabode M., Kah P., Martikainen J. (2013) Aluminium alloys welding processes: Challenges, joint types and process selection. *J. Eng. Manufacture*, 227: 1129–1137. <https://doi.org/10.1177/0954405413484015>
2. Boczekal S., Mitka M., Hrabia-Wiśnios O., et al. (2025) Analysis of the Structure and Properties of Welded Joints Made from Aluminum Alloys by Electron Beam Welding (EBW) and Friction Stir Welding (FSW). *Crystals*, 15 (3): 208. <https://doi.org/10.3390/cryst15030208>
3. Verma P., Kumar Lila M. (2021) A short review on aluminium alloys and welding in structural applications. *Materialstoday: Proceeding*, 46(20): 10687–10691. <https://doi.org/10.1016/j.matpr.2021.01.447>
4. Polmear I. J. (2006) Light Alloys: From Traditional Alloys to Nanocrystals – Fourth edition. Isevier Butterworth-Heinemann, Linacre House, Jordan Hill, Oxford, OX2 8DP, UK: 421.
5. Hatch J.E. (1984) Aluminum: Properties and Physical Metallurgy. ASM International: 424.
6. Ali S.; Agrawal A.P.; Ahamad N.; Singh T.; Wahid A. (2022) Robotic MIG welding process parameter optimization of steel EN24T. *Materialstoday: Proceeding*, 62, 239–244. <https://doi.org/10.1016/j.matpr.2022.03.091>
7. Cui S., Yu Y., Ma R., et al. (2023) Study on Morphology, Microstructure and Properties of 6063-T6 Aluminum Alloy Joints in MIG Welding. *Materials*, 16(13):4886. <https://doi.org/10.3390/ma16134886>
8. Yang K. Fei W., Liu H. (2021) Double-Pulse Triple-Wire MIG Welding of 6082-T6 Aluminum Alloy: Process Characteristics and Joint Performances. *Metals*, 11(9): 1388. <https://doi.org/10.3390/met11091388>
9. Han S.G., Zheng S.D., Cai D.T., et al. (2017) Microstructure Characteristics and Properties of 1561 Aluminum Alloy Weldments Processed by Different MIG Welding. *Materials Science Forum*, 893: 163–168. <https://doi.org/10.4028/www.scientific.net/MSF.893.163>
10. Wahid M.A., Siddiquee A.N., Khan, Z.A. (2020) Aluminum alloys in marine construction: characteristics, application, and problems from a fabrication viewpoint. *Marine Systems & Ocean Technology*, 15: 70–80. <https://doi.org/10.1007/s40868-019-00069-w>
11. Chen B.-Q., Liu K., Xu S. (2024) Recent Advances in Aluminum Welding for Marine Structures. *Journal of Marine Science and Engineering*, 12(9): 1539. <https://doi.org/10.3390/jmse12091539>
12. Sevim I., Hayat F., Kaya Y. et al. (2013) The study of MIG weldability of heat-treated aluminum alloys. *The International Journal of Advanced Manufacturing Technology*, 66: 1825–1834. <https://doi.org/10.1007/s00170-012-4462-z>
13. Kulkarnia S., Konnur V., Ganjigatti J. (2022) Optimization of MIG Welding Process Parameters with Grey Relational Analysis for Al 6061 Alloy. *Welding International*, 329: 387–393. <https://doi.org/10.1080/09507116.2022.2087569>
14. Lin H.L., Chen G.C., Cheng C.M. (2022) Effects of plasma-MIG hybrid welding parameters on performance and hot cracking susceptibility of 5083 Al alloy butt-joint welds. *The International Journal of Advanced Manufacturing Technology*, 122: 4055–4064. <https://doi.org/10.1007/s00170-022-10159-6>
15. Song G., Wang Z., Fan X., Liu L. (2023) Research Progress of Aluminum Alloy Welding/Plastic Composite Forming Technology in Achieving High-Strength Joints. *Materials*, 16(24): 7672. <https://doi.org/10.3390/ma16247672>
16. Korzhyk V., Gao S., Khaskin V., et al. (2025) Influence of speed and heat input of the pulsed-arc welding process on the structure formation of Al–Mg–Mn aluminum alloy joints. *Advances in Science and Technology Research Journal*, 19(8): 313–331. <https://doi.org/10.12913/22998624/205691>
17. Skorokhod A.Z., Sviridova I.S., Korzhik V.N. (1995) The effect of mechanical pretreatment of polyethylene terephthalate powder on the structural and mechanical properties of coatings made from it. *Mechanics of Composite Materials*, 30(4): 328–334. <https://doi.org/10.1007/BF00634755>
18. Mohammadtaheri M. (2012) A New Metallographic Technique for Revealing Grain Boundaries in Aluminum Alloys. *Metallography Microstructure and Analysis*, 1: 224–226. <https://doi.org/10.1007/s13632-012-0033-9>
19. Čičo P., Kalincová D., Kotus M. (2011) Influence of welding method on microstructural creation of welded joints. *Research in Agricultural Engineering*, 57 (Special Issue). <http://dx.doi.org/10.17221/57/2010-RAE>

20. Fialko N., Dinzhos R., Sherenkovskii J., et al. (2021) Establishing patterns in the effect of temperature regime when manufacturing nanocomposites on their heat-conducting properties. *Eastern-European Journal of Enterprise Technologies*, 4(5(112)): 21–26. <http://dx.doi.org/10.15587/1729-4061.2021.236915>
21. Akca E., Trgo E. (2015) Metallographic procedures and analysis – A review. *Periodicals of Engineering and Natural Sciences (PEN)*, 3(2): 9–11. <https://doi.org/10.21533/pen.v3i2.51>
22. Yasuda K. (1991) MIG welding of aluminium alloys. *Welding International*, 5(8): 614–617. <https://doi.org/10.1080/09507119109446786>
23. Lu Y., Zhu S., Zhao Z., Chen T., Zeng J. (2020) Numerical simulation of residual stresses in aluminium alloy welded joints. *Journal of Manufacturing Processes*, 50: 380–393. <https://doi.org/10.1016/j.jmapro.2019.12.056>
24. Nie J., Meng X.-F., Shi Y. (2011) Study on evaluation method of aluminum alloy pulse MIG welding stability based on arc voltage probability density. *Journal of Signal and Information Processing*, 2(3): 159–164. <https://doi.org/10.4236/jsip.2011.23020>
25. Borisov Yu.S., Kunitskii Yu.A., Korzhik V.N., et al. (1986) Yaprakova M.G. Structure and some physical properties of plasma-sprayed coatings of thenickel boride NiB. *Soviet Powder Metallurgy and Metal Ceramics*, 25(12): 966–969.
26. Wu L., Han X., Wu X., et al. (2022) The study of high-speed MIG welding assisted by compound external magnetic fields for 6N01-T6 aluminum alloy. *Journal of Manufacturing Processes*, 83: 576–589. <https://doi.org/10.1016/j.jmapro.2022.09.028>
27. Pépe N., Egerland S., Colegrove P. A., et al. (2011) Measuring the process efficiency of controlled gas metal arc welding processes. *Science and Technology of Welding and Joining*, 16(5): 412–417. <https://doi.org/10.1179/1362171810Y.000000002>
28. ISO 10042:2018. Welding – Arc-welded joints in aluminium and its alloys — Quality levels for imperfections. Access mode: <https://www.iso.org/standard/70566.html>